

Hydrogen molecule ion: Path-integral Monte Carlo approach

I. Kylänpää, M. Leino, and T. T. Rantala

Institute of Physics, Tampere University of Technology, P.O. Box 692, FI-33101 Tampere, Finland

(Received 17 August 2007; published 15 November 2007)

The path-integral Monte Carlo approach is used to study the coupled quantum dynamics of the electron and nuclei in hydrogen molecule ion. The coupling effects are demonstrated by comparing differences in adiabatic Born-Oppenheimer and nonadiabatic simulations, and inspecting projections of the full three-body dynamics onto the adiabatic Born-Oppenheimer approximation. Coupling of the electron and nuclear quantum dynamics is clearly seen. The nuclear pair correlation function is found to broaden by $0.040a_0$, and the average bond length is larger by $0.056a_0$. Also, a nonadiabatic correction to the binding energy is found. The electronic distribution is affected less than the nuclear one upon inclusion of nonadiabatic effects.

DOI: [10.1103/PhysRevA.76.052508](https://doi.org/10.1103/PhysRevA.76.052508)

PACS number(s): 31.15.Kb, 31.50.Gh

I. INTRODUCTION

There are a number of phenomena in molecular and chemical physics which are influenced by the quantum behavior of both nuclei and electrons, rovibrational dynamics being a good example; see Refs. [1–3] and references therein. In case of light-mass nuclei, protons in particular, treatment of the quantum nature of the nuclei is essential [4–6]. This has proven to be important in a description of the hydrogen bond, for example [7].

The hydrogen molecule ion (H_2^+), being the simplest molecule, has been studied extensively [8], and it has often been used as an example or a test case for an improved method or accuracy [9–14]. In addition to the free molecule, H_2^+ influenced by an electric or magnetic field is a well studied subject [15–21]. Furthermore, there is interest in descriptions that are not restricted to Born-Oppenheimer (BO) or other adiabatic approximations [22–28]. Such extensions can be easily realized by using quantum Monte Carlo (QMC) methods [29,30], for example.

Among the QMC methods the path-integral MC (PIMC) formalism offers a finite-temperature approach together with a transparent tool to trace the correlations between the particles involved. Though computationally extremely demanding, with some approximations it is capable of treating low-dimensional systems, such as small molecules or clusters accurately enough. Some examples found in the literature are H [31], HD^+ , and H_3^+ [32] and H_2 clusters [33–37] with special attention laid on 4He [38–42]. The approximations in these approaches relate to *ad hoc*-type potentials describing the interactions between particles.

In this work we evaluate the density matrix of the full three-body quantum dynamics in a stationary state and finite temperature. This is what we call “all-quantum” (AQ) simulations. Second, the electronic part only is evaluated as a function of internuclear distance in the spirit of the BO approximation, and third, the adiabatic nuclear dynamics is evaluated in the BO potential curve. These allow us to demonstrate the nonadiabatic electron-nuclei coupling by a projection of the AQ dynamics onto the adiabatic approximations.

We need to approximate the $-1/r$ Coulomb potential of electron-nucleus interactions at short range to make the

calculations feasible. We realize this with a carefully tested pseudopotential (PP). Also, the absent (ortho) or negligible (para) exchange interaction of nuclei is not taken into account. Finally, we want to emphasize that our purpose is to simulate a finite-temperature mixed state including correlations exactly, which is a challenging task for other methods. However, if high-accuracy zero-kelvin computations are preferred, one should turn to other methods such as the variational Monte Carlo (VMC) method, for example. For convenience, we have chosen 300 K, which essentially, but not exactly, restricts the system to its electronic ground state.

We begin with a brief introduction to the theory and methods in the next section. This includes a description of the PP and tools and concepts for the analysis in the following section. Then we carry on to the results. Throughout the paper atomic units are used: hartrees (E_H) for energies and Bohr radius (a_0) for distances.

II. THEORY AND METHODS

For a quantum many-body system in thermal equilibrium the partition function contains all the information of the system [43]. The local thermodynamical properties, however, are included in the density matrix from which all the properties of the quantum system may be derived [44]. The nonadiabatic effects are directly taken into account in the PIMC approach. In addition, finite-temperature and correlation effects are exactly included.

A. Path-integral Monte Carlo approach

According to the Feynman formulation of statistical quantum mechanics [45] the partition function for interacting distinguishable particles is given by the trace of the density matrix,

$$Z = \text{Tr} \hat{\rho}(\beta) = \lim_{M \rightarrow \infty} \int dR_0 dR_1 dR_2 \cdots dR_{M-1} \prod_{i=0}^{M-1} e^{-S(R_i, R_{i+1}; \tau)}, \quad (1)$$

where $\hat{\rho}(\beta) = e^{-\beta \hat{H}}$, S is the action, $\beta = 1/k_B T$, $\tau = \beta/M$, and $R_M = R_0$. M is called the Trotter number, and it characterizes the accuracy of the discretized path. In the limit $M \rightarrow \infty$ we

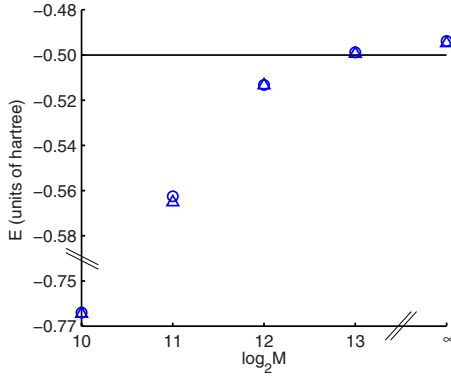


FIG. 1. (Color online) Hydrogen atom total energies with different Trotter numbers: infinite nuclear mass (triangles) and AQ (circles). Extrapolated ground-state energies are $-0.4947(1)E_H$ and $-0.4938(3)E_H$ for infinite nuclear mass and AQ simulations, respectively.

are ensured to get the correct partition function Z , but in practice sufficient convergence at some finite M is found, depending on the steepness of the Hamiltonian \hat{H} .

In the primitive approximation scheme of the PIMC formalism the action is written as [46]

$$S(R_i, R_{i+1}; \tau) = \frac{3N}{2} \ln(4\pi\lambda\tau) + \frac{(R_i - R_{i+1})^2}{4\lambda\tau} + U(R_i, R_{i+1}; \tau), \quad (2)$$

where $U(R_i, R_{i+1}; \tau) = \frac{\tau}{2}[V(R_i) + V(R_{i+1})]$ and $\lambda = \hbar^2/2m$.

Sampling of the configuration space is carried out using the Metropolis procedure [47] with the bisection moves [48]. This way the kinetic part of the action is sampled exactly and only the interaction part is needed in the Metropolis algorithm. The level of the bisection sampling ranges from 3 to 6 in our simulations, respectively with the increase in the Trotter number. The bisection sampling turns out to be essential with large Trotter numbers to achieve feasible convergence, for nuclei in particular. Total energy is calculated using the virial estimator [49].

B. Extrapolation of expectation values

The Trotter scaling procedure [32] for expectation values is used to obtain estimates for energetics in the limit $M \rightarrow \infty$. To use this procedure one needs expectation values with several different Trotter numbers. For the Trotter number M the scaling scheme is

$$\langle \hat{A} \rangle_\infty = \langle \hat{A} \rangle_M + \sum_{i=1}^N \frac{c_{2i}}{M^{2i}}, \quad (3)$$

where coefficients c_{2i} are constants for a given temperature and N represents the order of extrapolation. In this paper $N=2$ has been used for the energies of H_2^+ , and $N=3$ for hydrogen atom energies; see Figs. 1 and 2.

C. Pseudopotential of the electron

For the hydrogen molecule ion the potential energy is

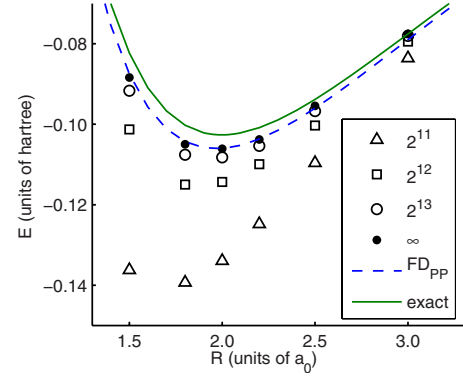


FIG. 2. (Color online) H_2^+ potential curves with different Trotter numbers $M=2^{11}$ (squares), $M=2^{12}$ (triangles), $M=2^{13}$ (circles), extrapolated values (dots), and finite-difference calculations with the pseudopotential (dashed line) and with exact e^-p^+ potential (solid line).

$$V(\mathbf{r}_1, \mathbf{r}_2, \mathbf{R}) = -\frac{1}{r_1} - \frac{1}{r_2} + \frac{1}{R}, \quad (4)$$

where $r_i = |\mathbf{r} - \mathbf{R}_i|$ and $R = |\mathbf{R}_1 - \mathbf{R}_2|$, \mathbf{r} being the coordinates of the electron and R the internuclear distance. Equation (4) sets challenges for the PIMC approach arising from the singularity of the attractive Coulomb interaction [50,51], which in this work is replaced by a PP of the form [52]

$$V_{PP}(r) = -\frac{\text{erf}(\alpha_c r)}{r} + (a + br^2)e^{-ar^2}. \quad (5)$$

The parameters $\alpha_c = 3.8638$, $\alpha = 7.8857$, $a = 1.6617$, and $b = -18.2913$ were fitted using direct numerical solution to give the exact ground-state energy of hydrogen atoms and the wave function accurately outside a cutoff radius of about $0.6a_0$. Also, a number of lowest-energy orbitals of the hydrogen atom are obtained accurately outside the same cutoff radius [53]. Because the bond length of H_2^+ is about $2a_0$, it is expected that bonding of the hydrogen molecule ion becomes properly described.

Hydrogen atom reference energies for different Trotter numbers are shown in Fig. 1, where triangles are obtained from infinite nuclear mass and circles are from AQ simulations. Extrapolated ground-state values are $-0.4947(1)E_H$ and $-0.4938(3)E_H$ for infinite nuclear mass and AQ simulations, respectively, statistical standard error of mean (SEM) given as the uncertainty in parentheses. We can note that within the 2SEM limits the proportion of these energies 0.9982 reproduces that of the Rydberg constants, $R_H/R_\infty = 0.9995$.

D. Spectroscopic constants

Within the BO approximation of diatomic molecules the corrections to electronic energies due to rovibrational motion of the nuclei can be evaluated from a Dunham polynomial [54]

$$E_{vJ} = -D_e + \omega_e \left(v + \frac{1}{2} \right) - \omega_e x_e \left(v + \frac{1}{2} \right)^2 + B_e J(J+1) - \alpha_e J(J+1) \left(v + \frac{1}{2} \right) + \dots, \quad (6)$$

where v and J are vibrational and rotational quantum numbers, respectively, and B_e , ω_e , $\omega_e x_e$, and α_e are the spectroscopic constants.

The spectroscopic constants of H_2^+ and D_2^+ are obtained as introduced in Ref. [54]. In atomic units,

$$B_e = \frac{1}{2I} = \frac{1}{2\mu R^2}, \quad (7)$$

$$\omega_e = \left(\frac{1}{\mu} \frac{d^2 E}{dR^2} \right)^{1/2}, \quad (8)$$

$$\omega_e x_e = \frac{1}{48\mu} \left[5 \left(\frac{d^3 E/dR^3}{d^2 E/dR^2} \right)^2 - 3 \frac{d^4 E/dR^4}{d^2 E/dR^2} \right], \quad (9)$$

$$\alpha_e = - \frac{6B_e^2}{\omega_e} \left[\frac{R d^3 E/dR^3}{3 d^2 E/dR^2} + 1 \right]. \quad (10)$$

Instead of determining these constants at the equilibrium distance only, as in Ref. [54], we evaluate expectation values from the distribution of nuclei, e.g., for the rotational constant

$$B_e = \frac{1}{2\mu} \int g(R) \frac{1}{R^2} dR, \quad (11)$$

where the pair correlation function $g(R)$ is normalized to unity. The other constants, Eqs. (8)–(10), are evaluated similarly.

E. Centrifugal distortion

The effects caused by the centrifugal distortion, arising from rotational motion of the nuclei, on the equilibrium distance can be assessed by inspecting the extremum values of the energy of the harmonic oscillator in rotational motion: $E_J(r) = \frac{1}{2}k(r-r_e)^2 + J(J+1)/2\mu r^2$. We find an approximate equation

$$\Delta R = \frac{4B_e}{\mu\omega_e^2 R_e^2} J(J+1), \quad (12)$$

where R_e is the equilibrium distance. Equation (12), however, does not include the anharmonic effects shown in Eq. (6), which evidently increase the bond length.

At finite temperature the rotational energy states should be weighted by the Boltzmann factor, which leads to

$$\Delta R = \frac{4B_e}{\mu\omega_e^2 R_e^2} \frac{\sum_J J(J+1) \exp[-\beta B_e J(J+1)]}{\sum_J \exp[-\beta B_e J(J+1)]}, \quad (13)$$

where $J=0, 1, 2, \dots$. Using the spectroscopic constants from Ref. [54] (see Table I) and temperature of 300 K we obtain

TABLE I. Expectation values of spectroscopic constants, Eqs. (7)–(11). A Morse potential [55] fitted to the FD_{PP} potential curve is used in the evaluation of the energy derivatives. Corresponding pair correlation functions are shown in Fig. 3. The first two columns are adiabatic nuclear dynamics results, and AQ results are in the last column.

	H_2^+		D_2^+ (cm^{-1})	H_2^+ (AQ) (cm^{-1})	
	(hartree)	(cm^{-1})			
B_e	0.0001366	30.35	15.24	29.26	This work
	0.0001344	29.85705			Ref. [54]
ω_e	0.0104816	2328.96	1668.25	2229.77	This work
	0.0104201	2315.3		(2232) ^a	Ref. [54]
$\omega_e x_e$	0.0003552	78.92	35.33	90.73	This work
	0.0003029	67.3			Ref. [54]
α_e	6.445×10^{-6}	1.432	0.45	1.636	This work
	7.201×10^{-6}	1.600			Ref. [54]

^aMCDFT, nonadiabatic [28].

$\Delta R = 0.0043a_0$. This approximation will be compared to our direct evaluation, below.

III. RESULTS

We consider three different cases separately in order to demonstrate the nonadiabatic effects. First, the electronic part only is evaluated as a function of internuclear distance in the spirit of the BO approximation. Second, the adiabatic nuclear dynamics is evaluated in the BO potential curve. Finally, H_2^+ is treated fully nonadiabatically with the AQ simulation. These allow us to demonstrate the nonadiabatic electron-nuclei coupling by a projection of the AQ dynamics onto the adiabatic approximations. In addition, spectroscopic constants and isotope effects are looked into.

A. Adiabatic electron dynamics

Though the PP, Eq. (5), reproduces the hydrogen atom energy exactly, an error of $-0.00342E_{\text{H}}$ from the exact value $-0.10263E_{\text{H}}$ results in the binding of another proton to the form H_2^+ . This is demonstrated in Fig. 2, where potential curves of H_2^+ from finite-difference calculations with V_{PP} from Eq. (5) and exact $V(r) = -r^{-1}$ are shown.

Our PIMC energies with increasing Trotter number M and the extrapolation to $M=\infty$ using Eq. (3) are shown in the same figure. These indicate clearly that the Trotter number has to be at least 2^{13} in order to find the minimum of the potential curve at the nuclear separation $R=2.0a_0$. The extrapolated values are in good agreement with the potential curve FD_{PP} , and there is almost a perfect match at $R=2.0a_0$, where the value of the extrapolated dissociation energy is $0.1061(2)E_{\text{H}}$.

For larger nuclear separations than $3.5a_0$, however, we are not able to reproduce the potential curve with these Trotter numbers: we get a too weakly binding molecule. This is assumed to be a consequence of the electronic wave function becoming more delocalized as the internuclear distance in-

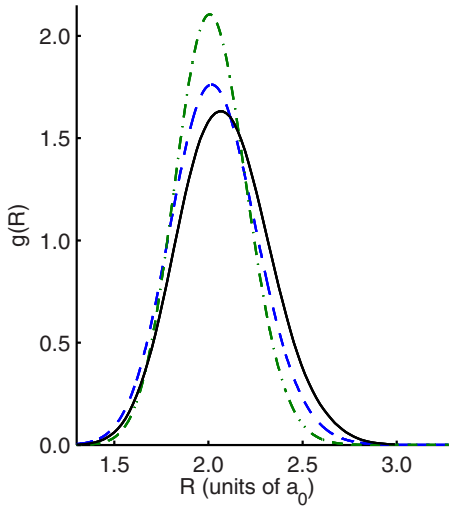


FIG. 3. (Color online) Nuclear pair correlation functions: H_2^+ AQ (solid line), H_2^+ QN (dashed line), and D_2^+ QN (dash-dotted line). The difference in the average nuclear separation between QN and AQ H_2^+ is $0.056(3)a_0$.

creases, and thus the “polymer ring” representing the electron is not capable of sufficient sampling of configuration space. This error should diminish with increasing M .

The electron-nucleus pair correlation function is shown in Fig. 4 and will be discussed below.

B. Adiabatic nuclear dynamics

For the quantum dynamics of the nuclei only (QN) we consider both H_2^+ and D_2^+ to see the isotope effect, too. The FD_{PP} potential curve in Fig. 2 is used, for which convergence with respect to Trotter number is found at $M \geq 2^6$ for both isotopes. The resulting pair correlation functions are shown in Fig. 3.

An average nuclear separation of $2.019(1)a_0$ for H_2^+ and $2.007(2)a_0$ for the isotope D_2^+ is found with $M \geq 2^6$. The full widths at half maximum (FWHM) of the pair correlation functions are $0.539(1)a_0$ and $0.454(1)a_0$ for these isotopes, respectively.

The difference in the bond length of H_2^+ between the adiabatic electron and adiabatic nuclei simulations—i.e., total distortion—is $0.019a_0$. The centrifugal contribution to this, the difference between one- and three-dimensional (1D and 3D) simulations of the nuclei, is $0.009(1)a_0$, which unexpectedly is about twice as much as the value $0.0043a_0$ evaluated from the approximate equation (13). The anharmonic contribution—i.e., difference between total and centrifugal distortions—is $0.010(1)a_0$. In Ref. [56] it was shown that anharmonic effects in H_2 molecules contribute about the same amount to total distortion as centrifugal force, which turns out to be the case here, too.

The difference between the total energies of the previous simulations (3D vs 1D) is $0.0009383(2)E_{\text{H}}$, which is close to $k_{\text{B}}T \approx 0.00095E_{\text{H}}$ as expected due to the presence of the two rotational degrees of freedom in 3D. The difference between the dissociation energies of adiabatic electron and nuclear

TABLE II. H_2^+ energetics (atomic units). The first three rows are BO and the next three are nonadiabatic values. For high-accuracy energetics see, for example, Ref. [14].

Method	E_{tot}	D_e	D_0^0	R
HF ^a	-0.6026	0.1026		2.000
VMC ^b	-0.6026	0.1026		2.000
PIMC ^c	-0.6061(2)	0.1061(2)	0.0997(1)	2.0
VMC ^c	-0.5971		0.0971	2.064
MCDFT ^d	-0.581		0.081	2.08
PIMC ^e	-0.59872(3)		0.09872(3)	2.075(2)

^aHartree-Fock [58].

^bVMC, Born-Oppenheimer [54].

^cVMC, nonadiabatic [30].

^dMCDFT, nonadiabatic (SAO) [28].

^eThis work.

simulations—i.e., the zero-point vibrational energy—is $0.0064(2)E_{\text{H}}$.

A Morse potential [55] fitted to the FD_{PP} potential curve is used in the evaluation of the spectroscopic constants; see Table I. This is justified because the nuclear simulations and analytical Morse wave function [57] calculations coincide. The spectroscopic constants of H_2^+ are close to those given in Ref. [54], which have been determined at the equilibrium distance of the nuclei, only. The same procedure is used for the spectroscopic constants of the other isotope. In Table I the same constants evaluated using the AQ instead of BO nuclear pair correlation function are also shown.

C. Nonadiabatic “all-quantum” dynamics

For H_2^+ the total energy of the AQ simulation with the Trotter number $M=2^{13}$ is $-0.60159(3)E_{\text{H}}$. The extrapolation procedure yields total energy $-0.59872(3)E_{\text{H}}$, which is only $0.0016E_{\text{H}}$ more binding than the value $-0.5971E_{\text{H}}$ from VMC simulations [30]. The zero-point energy obtained from simulations is $D_e - D_0^0 = 0.0074E_{\text{H}}$; see Table II. It should be pointed out that the error due to the pseudopotential in the AQ total energy is only about half of that found for the BO total energies.

The difference in dissociation energies of AQ and the 3D QN H_2^+ simulations is $0.00097E_{\text{H}}$, which is about $k_{\text{B}}T$, revealing additional electronic energy degrees of freedom in the first. AQ simulation for H_2^+ gives for the average nuclear separation $R=2.075(2)a_0$, which is $0.056a_0$ larger than that in the QN simulation. The AQ FWHM of the nuclear pair correlation function is $0.5785(2)a_0$, which shows a spreading of $0.040a_0$ compared to the QN results; see Fig. 3. With the Trotter number $M=2^{13}$ we find the AQ nuclear pair correlation function sufficiently converged.

In Fig. 4, BO and AQ electron-nucleus pair correlation functions are compared. AQ projection onto the BO bond length, $R=2.0a_0$, and BO results coincide, which indicates that the adiabatic BO approach for the electron dynamics is sufficient. Thus, it seems that the electron-nuclei coupling

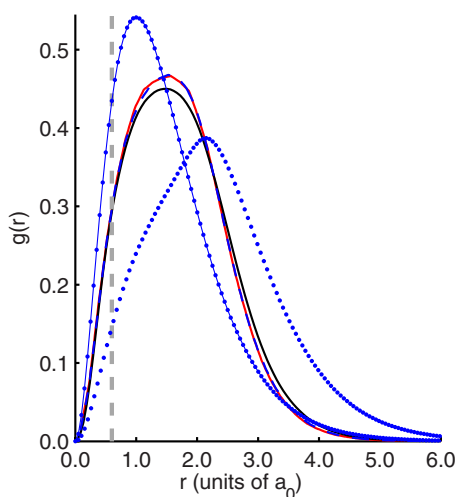


FIG. 4. (Color online) H_2^+ electron-nucleus pair correlation functions: AQ (solid line, second lowest curve), AQ projection to $R \approx 2.0a_0$ (solid line), and BO at $R=2.0a_0$ (dashed line). The latter two almost coincide. The dashed vertical line indicates the size of the pseudopotential core, $r=0.6a_0$. For comparison corresponding pair correlation functions for the hydrogen atom (dotted solid line) and H_2^+ (dotted line) obtained by using the analytical ground-state wave function of the hydrogen atom are also shown.

effects are more clearly seen in the dynamics of the nuclei; see Fig. 3. As one might expect, there is a noticeable difference between the AQ and BO electron-nucleus pair correlation functions due to varying bond length; see Fig. 4.

The AQ average nuclear separation is close to the value $2.064a_0$ obtained by a nonadiabatic VMC simulation [30]. The AQ pair correlation function of the nuclei (see Fig. 3) coincides with the scaled atomic orbital (SAO) one in Ref. [28] computed within the multicomponent density functional theory (MCDFT) scheme, not shown here.

All the spectroscopic constants in Table I are defined using the derivatives from a fitted Morse potential—i.e., BO potential energy surface. Thus, the “AQ spectroscopic constants” should be interpreted mainly as the direction of change in the values, except for B_e . The expectation values of the spectroscopic constants are obtained by weighting the equations by the nuclear pair correlation function from the corresponding simulation.

A projection of the AQ simulation to a potential curve of the nuclei is constructed with the help of the known solutions to the Morse potential. The distribution from the Morse wave function is fitted to the pair correlation function of the AQ simulation. The three-body system is then presented by an effective two-body potential. The projected potential curve shows clear differences in the dynamics of the nuclei between BO and AQ simulations; see Fig. 5. The minima of the potentials are set to zero: the difference in the dissociation energies between BO approach and AQ projection is about $0.036E_H$ and the shift in the equilibrium distance is $0.036a_0$. The spectroscopic constants with the projected potential curve are $B_e=29.26 \text{ cm}^{-1}$, $\omega_e=2047.94 \text{ cm}^{-1}$, $\omega_e x_e=78.12 \text{ cm}^{-1}$, and $\alpha_e=2.110 \text{ cm}^{-1}$. All this indicates that an effective Morse potential is not capable of describing nonadiabatic effects correctly.

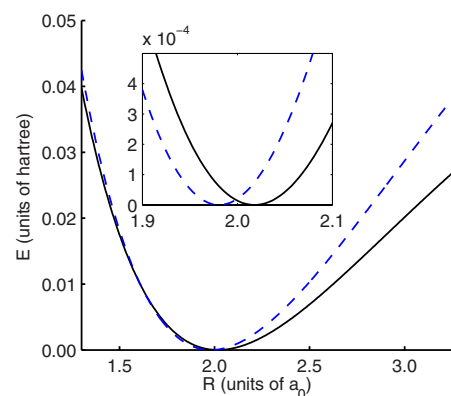


FIG. 5. (Color online) H_2^+ potential curves: Morse potential fitted to FD_{pp} (dashed line) and the effective Morse potential obtained from the projection of the AQ simulation (solid line); see the text for details. Corresponding nuclear pair correlation functions are shown in Fig. 3. The shift in the bond length is $0.036a_0$.

Finally, it may be of interest to see a visualization of the “polymer rings” representing the quantum particles in the PIMC simulation. So Fig. 6 presents the xy -plane (z -projection) snapshot from AQ simulation with Trotter number 2^{13} for all three particles. The “polymer ring” describing the electron is in the background and those of the nuclei are placed on top.

IV. CONCLUSIONS

The three-body quantum system, the hydrogen molecule ion (H_2^+), is reexamined, once again. The path-integral Monte Carlo method is used for evaluation of the stationary-state quantum dynamics. The PIMC method offers a finite-temperature approach together with a transparent tool to describe the correlations between the particles involved. We aim at tracing the electron-nuclei coupling effects in the three-body all-quantum—i.e., nonadiabatic—molecule. This is carried out by comparing the differences in adiabatic Born-Oppenheimer and AQ simulations and inspecting the projections from the AQ simulation onto the BO description

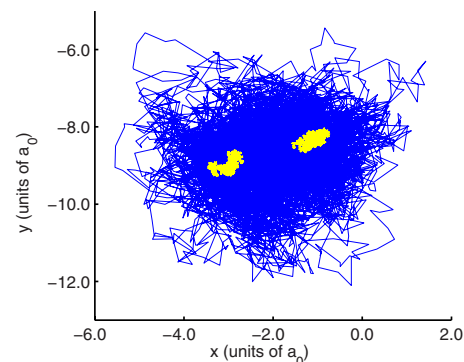


FIG. 6. (Color online) xy -plane (z -projection) snapshot from AQ simulation with Trotter number 2^{13} for all particles. The “polymer ring” describing the electron is in the background and those of the nuclei are placed on top.

of the electron-only and nuclear-only subsystems.

The approach turns out to be computationally demanding, but with the chosen pseudopotential for the attractive Coulomb potential and extrapolation to infinite Trotter number the task becomes feasible. By choosing low enough temperature, 300 K, we are able to compare our data to those from zero-kelvin quantum methods available in literature. Among others we have evaluated spectroscopic constants and molecular deformation, also considering the isotope effects.

With our fully basis set free, trial wave function free, and model free approach we are not able to compete in accuracy with the zero-kelvin benchmark values. However, due to the mixed-state density matrix formalism of the PIMC method, we are able to present the most transparent description of the particle-particle correlations.

Total energies from our simulations are more binding in nature compared to the benchmark values; see Table II. This is an expected effect of the pseudopotential in use; see Fig. 2 and FD_{pp} therein. The quantum dynamics of the system is well described, and distinct features of the coupling are ob-

served for the nuclei: a shift of $0.056a_0$ in the equilibrium bond length, increase of $0.040a_0$ in the width of the pair correlation function of the nuclei, and nonadiabatic correction of about $0.00097E_H$ to the dissociation energy. The electronic distribution is less influenced by the coupling than the nuclear one upon the inclusion of nonadiabatic effects; see Figs. 3 and 4.

The projection of the nonadiabatic three-body system with the help of Morse wave functions onto the two-body nuclei-only subsystem indicates that the Morse potential is not capable of describing nonadiabatic effects correctly; see Fig. 5.

ACKNOWLEDGMENTS

For financial support we thank the Graduate School of Tampere University of Technology and the Academy of Finland and for computational resources the facilities of Finnish IT Center for Science (CSC) and Material Sciences National Grid Infrastructure (M-grid, akaatti).

-
- [1] D. Marx and M. Parrinello, *J. Chem. Phys.* **104**, 4077 (1996).
 [2] T. Lopez-Ciudad, R. Ramirez, J. Schulte, and M. C. Böhm, *J. Chem. Phys.* **119**, 4328 (2003).
 [3] R. Ramirez, C. P. Herrero, and E. R. Hernández, *Phys. Rev. B* **73**, 245202 (2006).
 [4] H.-P. Cheng, R. N. Barnett, and U. Landman, *Chem. Phys. Lett.* **237**, 161 (1995).
 [5] M. Leino, J. Nieminen, and T. T. Rantala, *Surf. Sci.* **600**, 1860 (2006).
 [6] M. Leino, I. Kylänpää, and T. T. Rantala, *Surf. Sci.* **601**, 1246 (2007).
 [7] M. E. Tuckerman, D. Marx, M. L. Klein, and M. Parrinello, *Science* **275**, 817 (1997).
 [8] B. N. Dickinson, *J. Chem. Phys.* **1**, 317 (1933).
 [9] J. N. Silverman, D. M. Bishop, and J. Pipin, *Phys. Rev. Lett.* **56**, 1358 (1986).
 [10] L. Adamowicz and R. J. Bartlett, *J. Chem. Phys.* **84**, 4988 (1986).
 [11] H. W. Jones and B. Etemadi, *Phys. Rev. A* **47**, 3430 (1993).
 [12] J. H. Macek and S. Y. Ovchinnikov, *Phys. Rev. A* **49**, R4273 (1994).
 [13] V. V. Serov, B. B. Joulakian, D. V. Pavlov, I. V. Puzynin, and S. I. Vinitzky, *Phys. Rev. A* **65**, 062708 (2002).
 [14] V. I. Korobov, *Phys. Rev. A* **74**, 052506 (2006).
 [15] M. Vincke and D. Baye, *J. Phys. B* **18**, 167 (1985).
 [16] J. F. Babb and A. Dalgarno, *Phys. Rev. Lett.* **66**, 880 (1991).
 [17] K. T. Tang, J. P. Toennies, and C. L. Yiu, *J. Chem. Phys.* **94**, 7266 (1991).
 [18] U. Kappes and P. Schmelcher, *Phys. Rev. A* **53**, 3869 (1996).
 [19] A. Bouferguene, C. A. Weatherford, and H. W. Jones, *Phys. Rev. E* **59**, 2412 (1999).
 [20] R. E. Moss, *Phys. Rev. A* **61**, 040501(R) (2000).
 [21] C. Amovilli and N. H. March, *Int. J. Quantum Chem.* **106**, 533 (2006).
 [22] A. K. Bhatia and R. J. Drachman, *Phys. Rev. A* **59**, 205 (1999).
 [23] J. M. Taylor, A. Dalgarno, and J. F. Babb, *Phys. Rev. A* **60**, R2630 (1999).
 [24] V. I. Korobov, *Phys. Rev. A* **63**, 044501 (2001).
 [25] R. E. Moss and L. Valenzano, *Mol. Phys.* **64**, 649 (2002).
 [26] Y. Ohta, J. Maki, H. Nagao, H. Kono, and Y. Fujimura, *Int. J. Quantum Chem.* **91**, 105 (2003).
 [27] T. Kreibich and E. K. U. Gross, *Phys. Rev. Lett.* **86**, 2984 (2001).
 [28] T. Kreibich, R. van Leeuwen, and E. K. U. Gross, e-print arXiv:cond-mat/0609697.
 [29] C. A. Traynor, J. B. Anderson, and B. M. Boghosian, *J. Chem. Phys.* **94**, 3657 (1991).
 [30] D. Bressanini, M. Mella, and G. Morosi, *Chem. Phys. Lett.* **272**, 370 (1997).
 [31] X.-P. Li and J. Q. Broughton, *J. Chem. Phys.* **86**, 5094 (1987).
 [32] L. Knoll and D. Marx, *Eur. Phys. J. D* **10**, 353 (2000).
 [33] M. P. Surh, K. J. Runge, T. W. Barbee, E. L. Pollock, and C. Mailhot, *Phys. Rev. B* **55**, 11330 (1997).
 [34] M. C. Gordillo, *Phys. Rev. B* **60**, 6790 (1999).
 [35] M. C. Gordillo and D. M. Ceperley, *Phys. Rev. B* **65**, 174527 (2002).
 [36] M. Boninsegni, *Phys. Rev. B* **70**, 125405 (2004).
 [37] J. E. Cuervo and P.-N. Roy, *J. Chem. Phys.* **125**, 124314 (2006).
 [38] F. F. Abraham and J. Q. Broughton, *Phys. Rev. Lett.* **59**, 64 (1987).
 [39] D. M. Ceperley, *Rev. Mod. Phys.* **67**, 279 (1995).
 [40] M. Pierce and E. Manousakis, *Phys. Rev. Lett.* **81**, 156 (1998).
 [41] M. Pierce and E. Manousakis, *Phys. Rev. B* **59**, 3802 (1999).
 [42] Y. Kwon and K. B. Whaley, *Phys. Rev. Lett.* **83**, 4108 (1999).
 [43] H. Kleinert, *Path Integrals in Quantum Mechanics, Statistics, Polymer Physics, and Financial Markets*, 3rd ed. (World Scientific, Singapore, 2004).
 [44] E. L. Pollock and D. M. Ceperley, *Phys. Rev. B* **36**, 8343

- (1987).
- [45] R. P. Feynman, *Statistical Mechanics* (Perseus Books, Reading, Massachusetts, 1998).
- [46] D. M. Ceperley, *Rev. Mod. Phys.* **67**, 279 (1995).
- [47] N. Metropolis, A. W. Rosenbluth, M. N. Rosenbluth, A. H. Teller, and E. Teller, *J. Chem. Phys.* **21**, 1087 (1953).
- [48] C. Chakravarty, M. C. Gordillo, and D. M. Ceperley, *J. Chem. Phys.* **109**, 2123 (1998).
- [49] M. F. Herman, E. J. Bruskin, and B. J. Berne, *J. Chem. Phys.* **76**, 5150 (1982).
- [50] J. M. Thijssen, *Computational Physics* (Cambridge University Press, Cambridge, England, 2000).
- [51] S. D. Ivanov, A. P. Lyubartsev, and A. Laaksonen, *Phys. Rev. E* **67**, 066710 (2003).
- [52] A. Dal Corso, A. Pasquarello, A. Baldereschi, and R. Car, *Phys. Rev. B* **53**, 1180 (1996).
- [53] I. Kylänpää, Master's thesis, Tampere University of Technology, 2006.
- [54] S. A. Alexander and R. L. Coldwell, *Chem. Phys. Lett.* **413**, 253 (2005).
- [55] P. M. Morse, *Phys. Rev.* **34**, 57 (1929).
- [56] J. Lounila and T. T. Rantala, *Phys. Rev. A* **44**, 6641 (1991).
- [57] D. ter Haar, *Phys. Rev.* **70**, 222 (1946).
- [58] J. Kobus, L. Laaksonen, and D. Sundholm, URL <http://scarecrow.lg.fi/num2d.html>